Research Article

Deletion of type VIII collagen reduces blood pressure, increases carotid artery functional distensibility and promotes elastin deposition

Amanda L. Mohabeer [a,d], Jeffrey T. Kroetsch [b,d,e], Meghan McFadden [c,d], Negin Khosraviani [a,d], Thomas J. Broekelmann [f], Guangpei Hou [a,d], Hangjun Zhang [b,d], Yu-Qing Zhou [c,d], Minyao Wang [a,d], Anthony O. Gramolini [b,d], Robert P. Mecham [f], Scott P. Heximer [b,d], Steffen-Sebastian Bolz [b,d,e] and Michelle P. Bendeck [a,d]*

***a* - Department of Laboratory Medicine and Pathobiology,** *University of Toronto, Toronto, ON, Canada*
***b* - Department of Physiology,** *Faculty of Medicine, University of Toronto, Toronto, Ontario, Canada*
***c* - Institute of Biomedical Engineering,** *University of Toronto, Toronto, Ontario, Canada*
***d* - Translational Biology and Engineering Program,** *Ted Rogers Centre for Heart Research, University of Toronto, Toronto, Ontario, Canada*
***e* - Toronto Centre for Microvascular Medicine at TBEP,** *University of Toronto, Toronto, Ontario, Canada*
***f* - Department of Cell Biology and Physiology,** *Washington University School of Medicine, St. Louis, MO, USA*

Correspondence to Michelle P. Bendeck: TBEP, University of Toronto, 661 University Ave, Rm. 1432, Toronto, ON M5G 1M1, Canada. *michelle.bendeck@utoronto.ca (M.P. Bendeck)*
https://doi.org/10.1016/j.mbplus.2021.100085

Abstract

Arterial stiffening is a significant predictor of cardiovascular disease development and mortality. In elastic arteries, stiffening refers to the loss and fragmentation of elastic fibers, with a progressive increase in collagen fibers. Type VIII collagen (Col-8) is highly expressed developmentally, and then once again dramatically upregulated in aged and diseased vessels characterized by arterial stiffening. Yet its biophysical impact on the vessel wall remains unknown. The purpose of this study was to test the hypothesis that Col-8 functions as a matrix scaffold to maintain vessel integrity during extracellular matrix (ECM) development. These changes are predicted to persist into the adult vasculature, and we have tested this in our investigation. Through our *in vivo* and *in vitro* studies, we have determined a novel interaction between Col-8 and elastin. Mice deficient in Col-8 ($Col8^{-/-}$) had reduced baseline blood pressure and increased arterial compliance, indicating an enhanced Windkessel effect in conducting arteries. Differences in both the ECM composition and VSMC activity resulted in $Col8^{-/-}$ carotid arteries that displayed increased crosslinked elastin and functional distensibility, but enhanced catecholamine-induced VSMC contractility. *In vitro* studies revealed that the absence of Col-8 dramatically increased tropoelastin mRNA and elastic fiber deposition in the ECM, which was decreased with exogenous Col-8 treatment. These findings suggest a causative role for Col-8 in reducing mRNA levels of tropoelastin and the presence of elastic fibers in the matrix. Moreover, we also found that Col-8 and elastin have opposing effects on VSMC phenotype, the former promoting a synthetic phenotype, whereas the latter confers quiescence. These studies further our understanding of Col-8 function and open a promising new area of investigation related to elastin biology.

Introduction

Large artery stiffness is a significant and independent predictor of cardiovascular disease [1], which results from the inability of conduit arteries to maintain their homeostatic function. Vascular homeostasis relies on elastic arteries to function as reservoirs for blood pressure and flow. These vessels are equipped with elasticity – expanding during cardiac systole and passively recoiling with diastole, to allow for distal propagation of blood to perfuse end-organs. Importantly, the extensibility of these elastic arteries enable large changes in volume with minimal change in pressure as blood is conducted in the arterial tree. This is known as the Windkessel effect and dampens the pulsatile pressures to reduce the strain on the heart and maximize diastolic perfusion of the arterioles and capillary beds [2]. This mechanical behaviour of the vessel is governed by the extracellular matrix (ECM): proteins predominantly synthesized and deposited by medial vascular smooth muscle cells (VSMCs). Elastin is a dominant component in the vessel wall, and elastic fibers confer extensibility to large arteries, whereas fibrillar collagen fibers provide tensile strength.

The role of non fibrillar collagens in the vessel wall is less well established, however they may be important contributors during the remodeling processes associated with disease. One such collagen is the network-forming collagen-VIII (Col-8). Col-8 is a matrix protein which forms hexagonal lattice structures in many tissues [3–5]. For example, it is abundantly expressed in the Descemet's membrane of the cornea, where it provides extensibility and resistance to compression [6,7]. The expression of Col-8 in the vessel wall can be described as classic fetal gene reprogramming. Col-8 is highly expressed by VSMCs during the embryonic stage of development but is reduced to constitutively low levels of expression in the normal adult vessel [8]. Col-8 is upregulated during the progression of cardiovascular disease, and previous studies have focused on its bioactive-signaling role. For example, during vessel injury, Col-8 is deposited as a provisional matrix to promote VSMC migration and outward vessel remodeling [8]. Furthermore, it is atheroprotective by promoting the formation of a thick collagen-rich fibrous cap to reduce the potential for plaque rupture [9]. Col-8 negatively regulates the small Rho GTPase RhoA in VSMCs, and $Col8^{-/-}$ VSMCs have increased RhoA activity, actin stress fibers and basal focal adhesions [10]. Importantly, Col-8 expression is increased in vessels that are aged [11], atherosclerotic [8,9,12], or elastin haploinsufficient [13] , conditions all characterized by large artery stiffening.

However, no studies to date have investigated the biophysical impact of Col-8 on the vessel wall. Since Col-8 serves as a provisional matrix, and is highly expressed during embryogenesis (preceding that of fibrillar collagens and elastin), this suggests Col-8 may be necessary for matrix deposition and organization during the development of elastic arteries. It is well established that proper assembly of elastic fibers is essential to vessel physiology, and Col-8 has been associated with the elastic fiber network. Elastic fiber synthesis involves nearly 30 different proteins including tropoelastin, microfibrillar proteins, lysyl oxidase (LOX) and fibulins [14]. Importantly, systemic deletions of elastin ($Eln^{-/-}$), LOX ($Lox^{-/-}$) or fibulin-4 ($Efemp2^{-/-}$) all result in mice that die at birth due to severe cardiovascular malformations [15]. Mice of all three genotypes present with detrimental elastic fiber defects, vessel tortuosity and wall thickening. $Eln^{-/-}$ mice suffer from arterial stenosis, whereas $Lox^{-/-}$ and $Efemp2^{-/-}$ mice develop ascending aortic aneurysms. A hallmark feature of each of the three knockout (KO) mouse models was that the transcript for Col-8 (*Col8a1*) was the most upregulated mRNA in arteries relative to arteries from control mice [15]. This dramatic upregulation of *Col8a1* in mice deficient in elastic fiber proteins suggests that the non-fibrillar collagen may be important to maintain vessel structure, and may be necessary for matrix deposition and organization. Despite this, the relationship between elastin and Col-8 has not been investigated. We propose that Col-8 functions as a matrix scaffold protein to support vessel integrity during conduit artery development, which persists as the structural composition of the vessel and impacts the physiology of the adult vasculature.

In these studies, we report for the first time a novel interaction between Col-8 and elastin. Mice deficient in Col-8 ($Col8^{-/-}$) had reduced blood pressure and increased functional distensibility of carotid arteries, indicating an enhanced Windkessel effect. Differences in both the ECM composition and VSMC activity resulted in a $Col8^{-/-}$ carotid artery that displayed increased diameter with pressure, but enhanced catecholamine-induced VSMC contractility. *In vitro* studies with VSMCs revealed that the absence of Col-8 increased tropoelastin mRNA and elastic fiber deposition in the ECM, which was attenuated after exogenous Col-8 treatment. These findings suggest a causative role for Col-8 in reducing mRNA levels of tropoelastin and the deposition of elastic fibers in the matrix.

Materials & methods

All chemicals and reagents were purchased from Sigma-Aldrich unless otherwise indicated.

$Col8^{+/+}$ and $Col8^{-/-}$ mice

All animal studies were performed in compliance with the Animal Ethics Committee at the Faculty of

Medicine, University of Toronto, and in agreement with the guidelines of the Canada Council on Animal Care. Mice with targeted deletion for the genes *Col8a1* and *Col8a2* ($Col8^{-/-}$) on the C57BL/6J background were generated by the laboratory of Dr. Bjorn Olsen (Harvard Medical School) as previously described [16] and provided to Dr. Michelle Bendeck. All comparisons were made to $Col8^{+/+}$ mice which served as controls. Mice were aged to six months, with free access to water and standard chow.

Blood pressure

Mice were anesthetized with 2% isoflurane with continuous administration via an anesthesia vaporizer. Post midline incision, the right common carotid artery was clamped at the heart proximal end, and catheterized with a 1.4 French Millar blood pressure probe (Millar Inc.; Houston, Texas), which was inserted into the carotid artery after the clamp was removed. The level of isoflurane was decreased to 1.5%, allowed to stabilize for 3 min. Then the level of isoflourane was decreased to 1%, and blood pressure measurements were computed from the average of recordings, corresponding to 1 min of readings. Mean arterial pressure (MAP) was calculated by 1/3 systolic blood pressure (SBP) + 2/3 diastolic blood pressure (DBP). Pulse pressure (PP) was calculated by SBP –DBP. Post euthanasia, the chest cavity was rapidly exposed, heart isolated and blotted to remove blood, and weighed. Next the kidneys were excised, freed of surrounding tissue and adipose and weighed. Tissue weights were normalized to body weight.

Echocardiography

Mice were anaesthetized with isoflurane (for induction: 5% of isoflurane in 100% oxygen for about 3 min; for maintenance: 1.5% in 100% oxygen) and positioned on an imaging stage, monitoring heart rate and maintaining body temperature at 37°C. Fur was removed from the chest using depilatory cream (Nair), and ultrasound gel was applied directly onto the skin. Imaging was performed with a Vevo 770 high frequency ultrasound imaging system with a transducer of 30 MHz (VisualSonics Inc.; Toronto, Ontario). Heart function parameters were determined as previously described in detail [17]. In brief, at the aortic orifice, the pulsed Doppler velocity waveform and diameter were measured to calculate global left ventricular function including stroke volume and cardiac output (CO). To determine left ventricular contractility, M−mode recording at the middle segment of the ventricle was made to measure end diastolic and end systolic dimensions to calculate fractional shortening.

Pressure myography

Mice were euthanized by CO_2 asphyxiation and the left common carotid artery was exposed by dissection. Suture was placed along the left common carotid artery from the origin at the aorta to the carotid bifurcation, and measured to determine the '*in vivo*' length of the carotid artery. The vessel was subsequently excised and measured again, to determine the '*ex vivo*' length. An *in vivo* stretch ratio was then calculated by dividing the *in vivo* length by the *ex vivo* length. The vessel was isolated and maintained in ice cold physiological 3-(N-morpholino) propanesulfonic acid (MOPS) buffered saline solution composed of: 145 mM NaCl, 4.7 mM KCl , 1.5 mM $CaCl_2{\cdot}2H_2O$, 1.17 mM $MgSO_4{\cdot}7H_2O$, 1.2 mM $NaH_2PO_4{\cdot}2H_2O$, 2 mM pyruvate, 0.02 mM EDTA, 3 mM MOPS, 5 mM glucose. All myography equipment, including the chambers, peristaltic pump, pressure servo control, video dimension analyzer, and temperature control were purchased from Living Systems Instrumentation (St Albans City, Vermont). The carotid artery was placed into the myograph chamber, filled with physiological MOPS (here after referred to as calcium containing MOPS). The volume of the myography bath was maintained at 5 ml throughout the experiment. The vessel was mounted onto custom-made stainless steel cannulae [18] and attached with 6–0 braided silk suture (Teleflex; Markham, Ontario). With the system closed to pressure (i.e. approximately 0 mmHg) the vessel was stretched appropriately based on the calculated *in vivo* stretch ratio. The carotid artery was then pressurized to 80 mmHg, and warmed up to 37°C for 30 min. To prevent hysteresis the vessel was preconditioned by increasing the pressure from 0 to 160 mmHg for three cycles prior to data acquisition. Vessel diameter was visualized with a Nikon TMS microscope (Nikon Instruments Inc.; Melville, New York) attached to CCTV camera (Panasonic Canada Inc.; Mississauga, Ontario) and displayed by a black and white video monitor. Diameters were determined with the video dimension analyzer, recorded with AcqKnowledge software (Biopac Systems Inc.; Goleta, California), and data was analyzed using Microsoft Excel.

Pressure-diameter curves were generated as follows. Vessels in calcium containing MOPS buffer were subjected to increasing pressure from 0 to 160 mmHg. Pressure was increased by 20 mmHg increments, and was held at each point for 1 min while external diameter was recorded. This was performed 1–2 times per vessel. The vessel was then returned to 80 mmHg and washed with calcium-free MOPS buffer (same as above except use 1 mM EDTA and omit $CaCl_2{\cdot}2H_2O$), for 30 min (6x for 5 min). The vessel was then subjected to pressure increase from 0 to 160 mmHg in the calcium-free MOPS buffer. This

was performed twice. Segmental distensibility was calculated by $((OD_H\text{-}OD_L)/OD_L/20)$ where OD_H is outer diameter at higher pressure, and OD_L is outer diameter at lower pressure. Averaged SBP and DBP for each genotype (Table 2 were used to determine distensibilities from each individual pressure-diameter curve. Functional distensibility was calculated by $((OD_{SBP}\text{-}OD_{DBP})/(SBP\text{-}DBP)/20)$, where OD_{SBP} is outer diameter at SBP and OD_{DBP} is outer diameter at DBP.

Some vessels were additionally treated with phenylephrine (PE) [P8155]. This was performed as an initial first step in calcium containing MOPS (followed by pressure-diameter curves as described above). The vessel was maintained at 80 mmHg and treated with increasing concentrations of PE from 10^{-8} to 10^{-3} M for three minutes at each concentration. PE wash-out was performed with calcium containing MOPS until the diameter was comparable to that prior to PE addition at 80 mmHg. Percent constriction was determined by ((baseline diameter at 80 mmHg calcium – diameter at [PE] calcium)/baseline diameter at 80 mmHg calcium free X 100).

Proteomic analyses

Sample preparation for proteomic analyses

Carotid arteries (left and right) were dissected out of $Col8^{+/+}$ or $Col8^{-/-}$ mice and snap frozen in liquid nitrogen and stored at −80°C until processed. Each biological replicate contained arteries from two mice. Samples were prepared and analyzed as previously described [19]. In brief, samples were suspended in 150 μL of 50% (v/v) trifluorethanol in 100 mM ammonium bicarbonate, sonicated, and incubated at 60 °C for 2 h. After reduction with 5 mM dithiothreitol for 30 min at 55 °C, samples were carbamidomethylated with 15 mM iodoacetamide for 30 min at room temperature in the dark. Protein concentration was determined by Bradford assay, and samples were diluted 1:5 with 100 mM ammonium bicarbonate. Two mM calcium chloride and 5 μg of Trypsin/Lys-C mix (Promega) were added to the samples for overnight digestion at 37 °C, followed by 2 h at 37 °C with an additional 2 μg of Trypsin/Lys-C. Digestion was quenched with 5% (v/v) formic acid, and samples were centrifuged at 10,000 *g* to clear aggregates. From each sample, 50 μg of protein digest was transferred to a new tube and desalted using OMIX C18 solid phase extraction tips (Agilent) per manufacturer's instructions. Desalted peptides were dried by vacuum centrifugation and reconstituted in 50 μL of 5% (v/v) formic acid.

LC-MS/MS data acquisition

Tryptic peptides were analyzed by reverse-phase liquid chromatography – tandem MS (LC-MS/MS) on an Easy-nLC 1200 coupled to a Q Exactive Plus mass spectrometer using a Nanospray Flex Ion Source [Thermo Fisher Scientific]. All experiments utilized two technical replicates per biological sample, applying a Top10 Data-Dependent Acquisition (DDA) methodology. A 5 μL sample was loaded onto a 10-cm in-house packed 75 μm i.d. column (Reprosil-Pur Basic C18, 3 μm, 100 Å; Dr. Maisch HPLC), and separated using a 2-hour acetonitrile linear gradient (2%–35% (v/v) in 0.1% (v/v) formic acid in HPLC-grade water) at a flowrate of 250 nl/minute. Full MS1 spectra were collected from 400 to 1500 *m/z* at 70,000 resolution for a maximum injection time of 100 msec with AGC target of $1e^6$, followed by 10 data-dependent MS2 spectra at a resolution of 17,500 and 55 msec maximum injection time with AGC target of $5e^5$. Normalized

Table 1 qRT-PCR primer sequences.

Gene	Forward 5′ → 3′	Reverse 5′ →3′
GAPDH	GACAACTTTGGCATTGTGGAAGG	ACCAGTGGATGCAGGGATGAT
COL1A1	CCCCGGCCCCATTGGTAACG	GAGGGACCAGGGGGACCGAC
COL2A1	ACGCGGACTCTGTTGCTGCT	GCGGGACCCCTTTGTCCACG
COL3A1	CCCGGGTGCTCCTGGACAGA	CACCCTGAGGACGCGGA
COL5A1	GGACTAGTCCGCTTTTCCCTGTCAACT	GTGGTCACTGCGGCTGAGGAACTT
COL5A2	TCGGGGCCTAAAGGAGGCCA	CCCCAGCACCCAAAGGC
COL5A3	TGCCACAGTCTCGCAGGGGT	CTGCTGCCCGGAACTTGGGG
COL8A1	AGAGTGCACCCAGCCCCAGT	TGGGTGGCACAGCCATCACATTT
COL8A2	CCTGCAGGCTCTGCCTGTCC	CACTCTTGGCCCACACCCCA
FN1	TACCAAGGTCAATCCACACCCC	CAGATGGCAAAAGAAAGCAGAGG
LOX	CATGGTGGGCGACGACCCCT	GGTCCGGGAGACCGTACTGGA
ELN	CTATGGAGGAGCCCTTGGAG	CACAGGATTTCCCAAAGCAG
FBN1	AATATCTCGGAGCCATTTGC	CAGGTCTACGGCAGTTGTCA
FBN2	TGCAAAATCAATGGCTACACC	CTCCAGGCTGATTTGCTCCT
FBLN5	CCAGTGTATCGAGGGCCTTA	CTGGTTGCCTTCATCCATCT
MAGP1	GCTGGCTCAGGGCCAATATG	GAGGACTCACTTCTTGGTAGTCA
EMILIN1	AGCACCCTCCACACCACT	CTGCTGCACCTTCTCTGAC
EFEMP2	ATGGCTATGAGTGGGATGCAGACAGCCAGC	TGGCAATAGCGGTAACGACACTCATCTATG

Table 2 Blood pressure, echocardiography and weight analyses of Col8$^{+/+}$ and Col8$^{-/-}$ mice.

Parameters	Col8$^{+/+}$	Col8$^{-/-}$	Significance
Blood Pressure (n = 8–11)			
Systolic (mmHg)	103 ± 3.8	87.0 ± 3.2	P = 0.00760
Diastolic (mmHg)	64.6 ± 2.2	57.0 ± 3.3	NS
Mean Arterial (mmHg)	77.1 ± 2.5	67.3 ± 3.1	P = 0.0239
Pulse Pressure (mmHg)	38.1 ± 2.6	30.0 ± 1.8	P = 0.0309
Heart Rate	465 ± 24	462 ± 20	NS
Echocardiography (n = 17–21)			
Cardiac Index (mL/min/g)	0.552 ± 0.024	0.516 ± 0.020	NS
LV stroke volume (μL)	44.7 ± 1.7	40.7 ± 1.6	NS
LV fractional shortening (%)	28.9 ± 1.3	27.5 ± 1.5	NS
Weights (n = 14–17)			
Body Weight (g)	33.7 ± 0.63	32.2 ± 0.76	NS
Heart percentage of body weight (%)	0.421 ± 0.0074	0.430 ± 0.011	NS
Kidney percentage of body weight (%)	1.38 ± 0.029	1.33 ± 0.06	NS

Values represent the mean ± SEM.

high energy collision-induced dissociation energy (NCE) was set at 28, dynamic exclusion was set to 30 sec, and only 2^+ to 5^+ charge states were included.

Database search and statistical analyses

RAW files were searched against the UniProt mouse FASTA database (updated October 2019) using MaxQuant software version 1.6.0.1 (Max Planck Institute of Biochemistry). Methionine oxidation, N-terminal acetylation, and asparagine or glutamine deamidation were selected as variable modifications, and cysteine carbamidomethylation as a fixed modification. False discovery rate (FDR) was set to 1% using a reversed-target decoy database. All raw files and search results are available from MassIVE with accession code: MSV000087422. All data visualization and statistical analyses were carried out using Perseus software version 1.6.2.1. Label-free quantification (LFQ) values [20] were Log_2-transformed and filtered to only include proteins with valid values in at least three of four biological replicates of at least one experimental group. To allow more meaningful statistics, missing values were imputed from a normal distribution, with a downshift of 1.8 and width of 0.3 standard deviations (Supplemental Figs. 1 & 2. Differential proteins were identified based on the threshold of $p < 0.05$, and hierarchical clustering and accompanying heat map were generated using normalized values across all samples for each protein.

Biochemical measurements of collagen and elastin

Protein, collagen and elastin content was determined according to Stoilov et al. [21]. Briefly, the carotid arteries were hydrolyzed at 105 °C in 25ul constant boiling 6 N HCl for 48 h, dried and then dissolved in 400ul distilled water. For total protein, 5ul and 20ul aliquots were assayed in duplicate by mixing with 100ul ninydrin working reagent. After 10 min of incubation at 85 °C the absorbance at 575 nm was read and protein content was determined after comparison to a known amino acid standard. The average standard error for the assays was 1.7%. Collagen content was determined after mixing 50ul sample in duplicate for 20 min at room temperature with 100ul chloramine T working solution followed by incubation with 100ul Erlich's solution for 20 min at 65 °C. Absorbance was read and hydroxyproline content determined by comparison with known hydroxyproline standards. Collagen content was calculated using 13.5% of collagen is hydroxyproline. The average standard error for this assay was 2.8%. Elastin was determined by competitive immuno-assay. In 5 sets of assays 2ul (n = 6), 4ul (n = 8), or 10ul (n = 4) samples were mixed with rabbit anti-desmosine at a final dilution of 1:2000 for 1 h at room temperature. The samples were then added to desmosine-ovalbumin coated plates overnight at 4 °C. After washing, bound antibody was detected using peroxidase labeled-goat anti-rabbit IgG [5220–0336; SeraCare] followed by Sure-Blue peroxidase substrate [5120–0075; SeraCare]. Absorbance at 650 nm was read and elastin content was determined using an elastin hydrolysate standard. The average standard error for this assay was 14.7%.

Cell culture of Col8$^{+/+}$ and Col8$^{-/-}$ VSMCs

Murine primary VSMCs were isolated from Col8$^{+/+}$ and Col8$^{-/-}$ mice as previously described [22]. In brief, VSMCs were harvested from carotid arteries after dispersion by elastase and

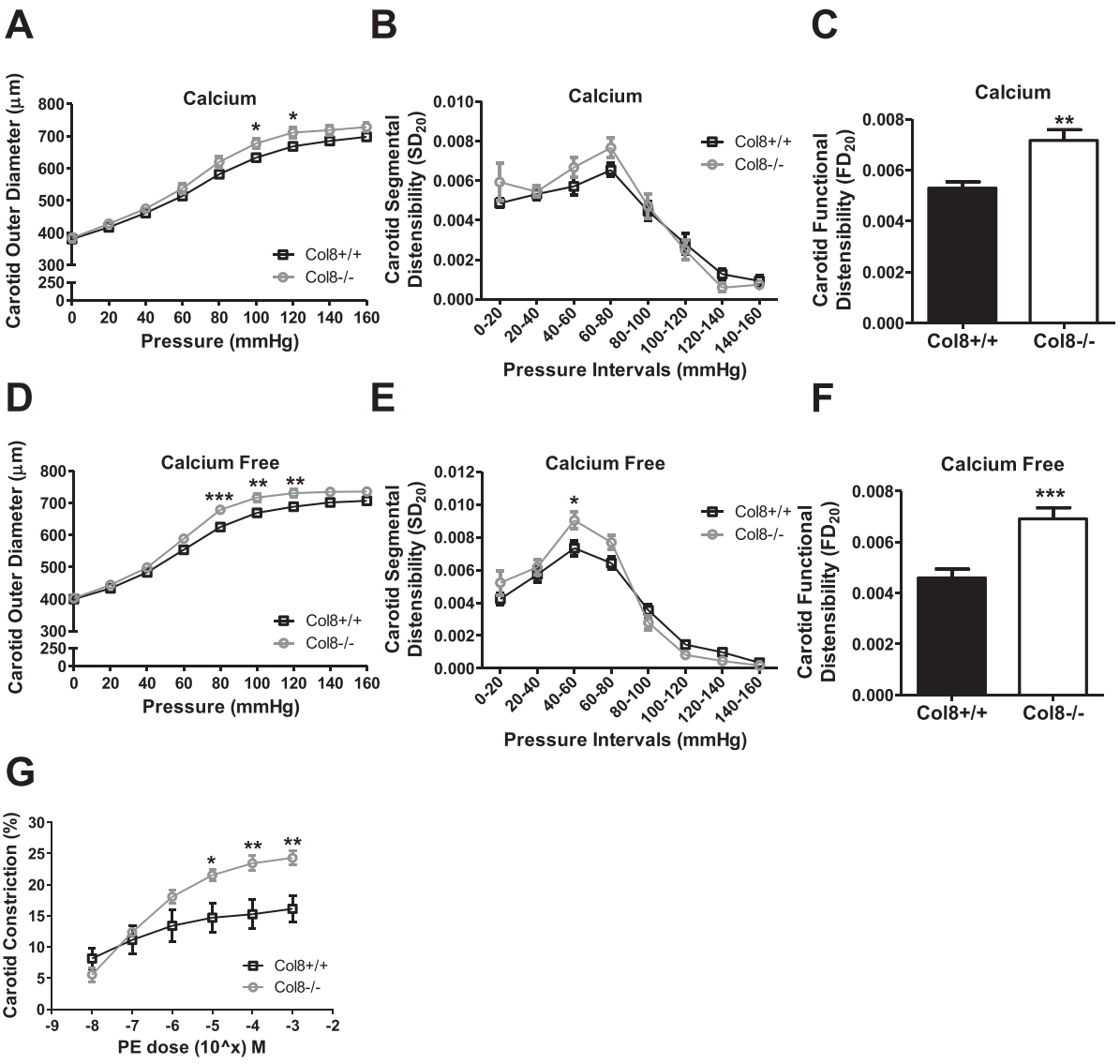

Fig. 1. Increased pressure-diameter curves, functional distensibility and phenylephrine-induced contractility in Col8$^{-/-}$ carotid arteries. A & D, Pressure myographs were obtained for carotid arteries maintained in either calcium or calcium-free MOPs buffer. Vessels were subjected to pressure increase from 0 to 160 mmHg, at 20 mmHg increments, and external diameter was recorded. **B & E**, Segmental distensibility and **C & F**, functional distensibility were calculated. **G**, Carotid arteries were maintained in calcium-containing MOPs buffer at 80 mmHg and subjected to increasing concentrations of PE from 10^{-8} M to 10^{-3} M. Changes in external diameter were recorded and percent constriction was calculated. Values represent the mean ± SEM. (A-F n = 8–11; G n = 5–8), *p < 0.05; **p < 0.01; ***p < 0.001.

collagenase treatments. Cells were cultured in Dulbecco's Modified Eagle Medium (DMEM) [11885084; Gibco] supplemented with 10% fetal bovine serum (FBS) [12483020; Thermo Fisher Scientific], 100 units/mL penicillin and 100 μg/mL streptomycin [15140122; Thermo Fisher Scientific Cells were maintained at 5% CO_2 and used between passages 5–8. Cells were seeded at 60,000 cells/well into 6-well plates and cultured for 12 days with media changes every second day. At post-confluence (day 4), cells were additionally treated with 50 μg/ml ascorbic acid every 24 h to promote collagen synthesis. This seeding setup was used for all subsequent cell culture experiments (qRT-PCR, immunofluorescence, immunoblotting).

Phenylephrine treatment for phosphorylation of MYPT1

In some experiments, cells were grown to day 12, serum starved for 24 h and treated with 10 μM PE

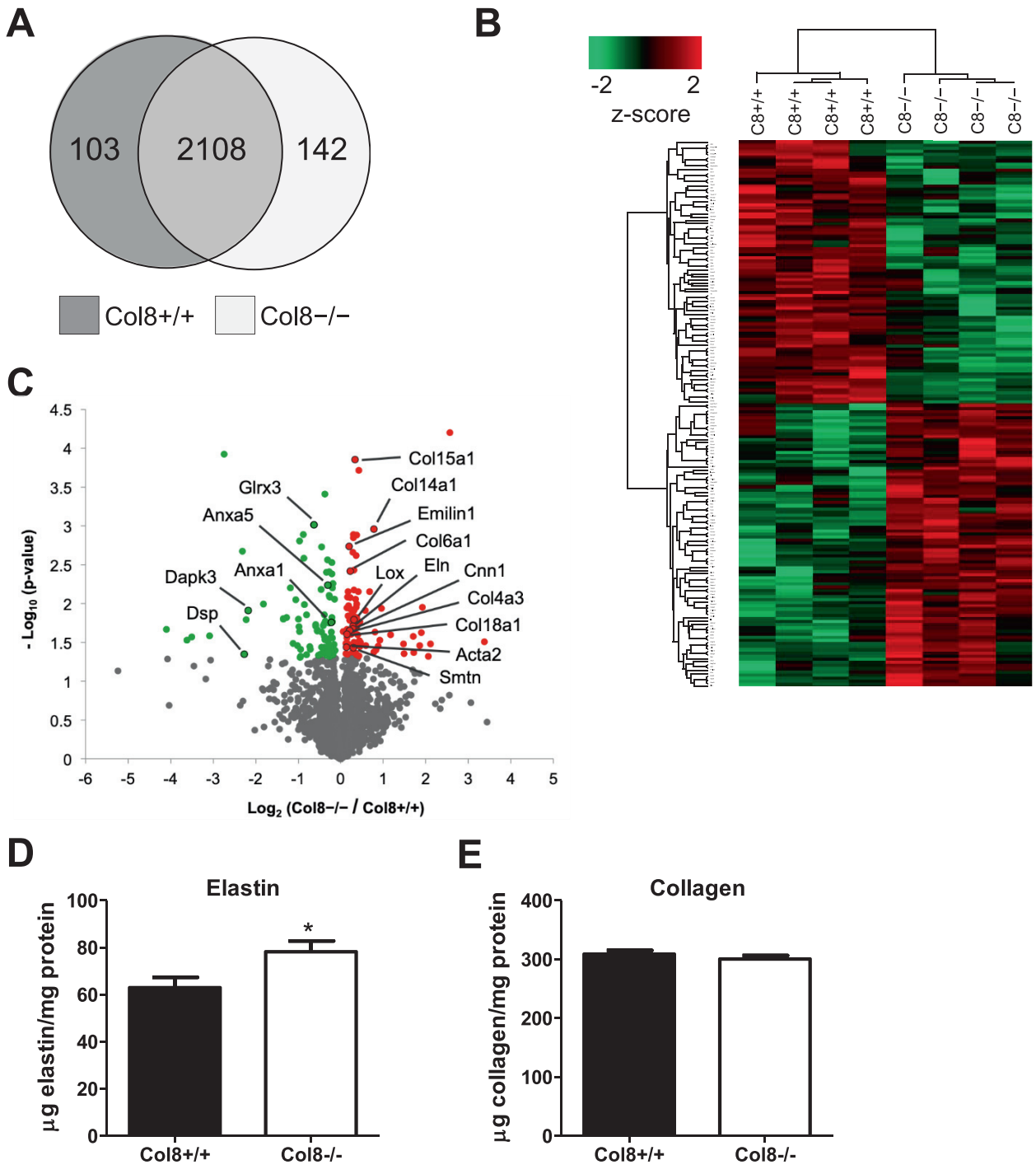

Fig. 2. Differential VSMC and extracellular matrix protein expression in Col8$^{+/+}$ and Col8$^{-/-}$ carotid arteries. **A**, Venn diagram illustrating the number of proteins shared by Col8$^{+/+}$ and Col8$^{-/-}$ carotid arteries in $\geq$ 3 biological replicates per group. **B**, Heat map depicting the hierarchical clustering of proteins significantly different($p < 0.05$). **C**, Volcano plot identifying differentially expressed VSMC and ECM proteins. **D**, elastin and **E**, collagen content were measured biochemically via desmosine and hydroxyproline assays respectively in Col8+/+ and Col8$^{-/-}$ carotid arteries. Values represent the mean ± SEM (A-C n = 4; for the proteomic studies each biological replicate contains the left and right carotid arteries pooled from 2 mice. We then used 4 biological replicates per genotype. D-E n = 9–12). *$p < 0.05$.

for 10 min in 1% FBS media. Cells were subsequently lysed and immunoblotted for phospho-myosin phosphatase target subunit 1 (MYPT1) and total MYPT1, as described below.

Exogenous rCol-8 treatment

In some experiments, cells were grown in wells pre-coated with exogenous recombinant Col-8 (rCol-8). Recombinant Col-8 was synthesized by and purchased from GenScript (Piscataway, New Jersey). In brief, a human *Col8a1* plasmid construct was amplified and prepared by maxi-prep and expressed in 293-6E cells 6-well plates coated with 2 μg/cm^2 exogenous rCol-8 in PBS overnight at 4 °C. Plates were washed twice with cold PBS before the addition of cells. Cells were grown to day 12 and immunofluorescently labeled for elastin (no decellularization) or harvested to measure tropoelastin mRNA levels. Both these procedures are described in detail below.

Quantitative real-time polymerase chain reaction (qRT-PCR)

Total RNA was harvested at day 12 with the Qiagen RNeasy Mini Plus Kit [74134]. Concentration and RNA purity were determined using a spectrophotometer [Nanodrop 1000, Thermo Fisher Scientific]. 1 μg of RNA was treated with DNAase I [18068–015, Invitrogen] and converted to cDNA using Superscript First-Strand Synthesis System [11904–018, Invitrogen] as per manufacturer's instructions. cDNA was mixed with Power SYBR Green PCR Master Mix [4367659, Invitrogen] and the appropriate primers for real time RT-PCR amplification. Primer sequences [23–28] are summarized in Table 1. Data was analyzed using Bio-Rad CFX Manager Software 3.0. Target gene expression was normalized to GAPDH and expressed as a fold change relative to wildtype control (Col8$^{+/+}$) samples via the 2^- ΔCt method [29].

Decellularization and immunofluorescence of ECM proteins

Cells were grown on 22x22mm micro cover glass (coverslips) [48366–067, VWR] placed into 6-well plates for 12 days to allow sufficient matrix deposition. Decellularization was performed prior to fixation and immunofluorescence staining. Cells were washed once with warmed (37 °C) PBS and then incubated with warmed decellularization buffer (0.25 M ammonium hydroxide in 25 mM Tris (pH 7.4)) for 30 min in the incubator [30]. The buffer was aspirated slowly with a Pasteur pipette to avoid disruption of the matrix. Treatment, incubation and removal of the decellularization buffer were repeated 2–3 times to ensure maximum removal of cells. Matrices were fixed with 100% ice cold methanol in the freezer (−20 °C) for 25 min. They were subsequently washed three times with 1x PBS and then incubated with 1% BSA in PBS for one hour at room temperature. Post washing, samples were incubated with primary antibody at 1:100 dilution overnight at 4 °C. Coverslips were incubated with the following antibodies: anti-mouse tropoelastin rabbit polyclonal [PR385, Elastin Products Company]; anti-mouse collagen-I rabbit polyclonal [ab21286, Abcam]; anti-mouse fibronectin rabbit polyclonal [ab23750, Abcam]. Post washing, coverslips were incubated with Alexa Fluor 488 goat anti-rabbit IgG [A-11008, Invitrogen] at 1:200 dilution one hour at room temperature. Prior to mounting, Hoechst 33,342 [H3570, Invitrogen] was added to label nuclei. Coverslips were mounted onto slides with ProLong Gold Antifade Mountant [P36930, Invitrogen], and imaged with an Olympus FV3000 Confocal Microscope with Fluoview FV31S-SW software (Olympus Canada Inc.; Richmond Hill, Ontario). Four regions of interest (ROI) per slide were imaged at 20x objective and z-stacks were acquired at 1.3 mm steps (9–11 slices). For quantitative analysis, the z-stack slices were collapsed a single Olympus image (OIR file format) with maximum intensity and converted to a TIFF file. The mean intensity of this image was then determined by the RGB (0,255,0) scale, and averaged amongst the four ROIs to give a value per sample.

Immunoblotting

Cells were harvested at day 12 in 1x cell lysis buffer [9803; Cell Signaling Technology] supplemented with 1 μM phenylmethylsulfonyl fluoride (PMSF). Protein concentration was measured using the DC Protein Assay [5000116; Bio-Rad]. Samples were diluted to equal protein concentration, mixed with 4x sample dilution buffer (200 mM Tris-HCl pH 6.8, 8% SDS, 40% glycerol, 4% β-mercaptoethanol, 0.08% bromophenol blue), boiled for 5 min at 100 °C , and resolved on10-15% SDS-PAGE gels. Gels were transferred onto PVDF membrane [162–0177; Bio-Rad] at 100 V for 1 h on ice and subsequently incubated with 5% skim milk powder in TBST (10 mM Tris, 150 mM NaCl, 0.5% Tween-20) for 1 h at room temperature. Membranes were incubated with the appropriate primary antibody (diluted in 1% BSA in TBST) overnight at 4°C. After washing, membranes were incubated with HRP-linked secondary antibody (diluted in 1% BSA in TBST) for 1 h at room temperature. Antibodies against the following proteins were purchased from Cell Signaling Technologies unless otherwise specified: anti-human α-SMA rabbit polyclonal [14968]; anti calponin-1 rabbit monoclonal [17819]; anti-human SM22-α rabbit polyclonal [ab155272, Abcam]; anti-bovine smooth muscle myosin heavy chain 11 (SM-MHC) rabbit

polyclonal [ab53219, Abcam]; anti-human phospo-MYPT1 rabbit polyclonal [5163]; anti-human rabbit polyclonal [2634]; anti-human β-actin rabbit polyclonal [4967]; anti-goat HRP-linked rabbit secondary made in goat [7074]. Blots were detected with enhanced chemiluminescence as per manufacture guidelines [NEL104001EA, Perkin Elmer], visualized with Chemi Doc Touch Imaging System [Bio-Rad] and analyzed by densitometry with Bio-Rad Image Lab Software. Restore Plus western blot Stripping Buffer [46430, Thermo Fisher Scientific] was used for reprobing. Calponin, SM22 and phospho-MYPT1 were probed first, followed by MHC, α-SMA and MYPT1 respectively. β-actin served as the loading control and was performed last.

Statistical analysis

Experimental data were analyzed by Student's unpaired *t*-test (comparing two groups). For myographs, Two-way ANOVA was utilized followed by Bonferroni's multiple comparison test. For all analyses, $p < 0.05$ are denoted by an asterisk (*), $p < 0.01$ by two asterisks (**), $p < 0.001$ by three asterisks (***) and are considered to be significant differences. For all statistical analyses, F tests were performed to compare variances and all populations were determined to be evenly distributed.

Results

Reduced blood pressure in Col8$^{-/-}$ mice

The relationship between arterial compliance and blood pressure is well established. Therefore, we measured blood pressure (BP) in Col8$^{+/+}$ and Col8$^{-/-}$ mice at six months of age. SBP, MAP, and PP were all decreased in Col8$^{-/-}$ mice (Table 2), with the latter potentially reflecting differences in arterial stiffness. To determine whether the hypotensive phenotype observed in the Col8$^{-/-}$ mice was due to a decrease in cardiac output (CO), echocardiography was performed. However, no differences were observed between the two genotypes for the left ventricular fractional shortening, stroke volume or cardiac index (CO normalized to body weight) (Table 2).

Pressure-diameter curves, functional distensibility and phenylephrine-induced contractility were increased in Col8$^{-/-}$ carotid arteries

Since MAP was decreased, but cardiac function was not altered, we next focused on determining the impact of Col-8 deletion in conduit arteries, since Col-8 expression is high in these arteries, and elastic vessel compliance can impact systolic blood pressure [31]. To delineate the individual factors (VSMCs, ECM, extrinsic factors) which contribute to vessel compliance, we performed *ex vivo* compliance testing on Col8$^{+/+}$ and Col8$^{-/-}$ carotid arteries. Vessels were maintained in either calcium or calcium-free MOPS buffer to determine both active (cell engagement) and passive (ECM only) vessel properties, respectively. Col8$^{-/-}$ carotids demonstrated increased diameter in response to pressure relative to Col8$^{+/+}$ carotid arteries under both calcium and calcium-free conditions (Fig. 1.A, D). In calcium MOPS buffer, significant differences were determined for the pressure range of 100–120 mmHg (100 mmHg: Col8$^{-/-}$ 677 ± 14 μm versus Col8$^{+/+}$ 633 ± 14 μm, $p < 0.05$), and the differences were even more pronounced between 80 and 120 mmHg for calcium-free conditions (100 mmHg: Col8$^{-/-}$ 716 ± 12 μm versus Col8$^{+/+}$ 668 ± 5 μm, $p < 0.05$). Segmental distensibility, which refers to the incremental changes in distensibility during each pressure step, was increased in Col8$^{-/-}$ arteries over the pressure interval 40–60 mmHg under calcium-free (Fig. 1.E) but not calcium conditions (Fig. 1.B). Functional distensibility refers to the measurement of distension with pressure applied corresponding to the normal physiological blood pressure of the mouse (as reported in Table 2). Since functional distensibility takes into account the physiological pressure, any differences here most closely reflect what the vessel would experience *in vivo* in the presence of calcium. Functional distensibility was elevated under both conditions in Col8$^{-/-}$ carotid arteries compared to Col8$^{+/+}$ (Fig. 1.C, F). These differences in this value was exacerbated in the absence of calcium, since only ECM integrity was evaluated, in the absence of any cellular contribution, which might serve to counteract distension with cell contraction. Since Col8$^{-/-}$ carotid arteries displayed differential pressure-diameter curves under calcium and calcium-free conditions, we hypothesized that the cells in the Col8$^{-/-}$ vessel may be more vasoactive/responsive to compensate. To test this, carotid arteries were stimulated with the vasoconstrictor PE. Col8$^{-/-}$ carotid arteries demonstrated greater constriction in response to PE compared to Col8$^{+/+}$ vessels beginning at the concentration of 10^{-5}M PE (Fig. 1.G). At maximum concentration of 10^{-3}M PE, Col8$^{-/-}$ vessels constricted 24.3 ± 1.1% versus Col8$^{+/+}$ arteries at 16.1 ± 2.1% constriction ($p < 0.01$).

Differential VSMC and extracellular matrix protein expression in Col8$^{+/+}$ and Col8$^{-/-}$ carotid arteries

To provide a greater depth of understanding about changes in protein expression, we conducted a global proteomic assay with Col8$^{+/+}$ and Col8$^{-/-}$ carotid arteries. Arteries were harvested from mice at six months of age, and

vessels from two mice represented one biological replicate. LC-MS/MS analyses identified a total of 2353 proteins with 2108 of these proteins shared by both genotypes, and100 and 142 proteins specific to Col8$^{+/+}$ or Col8$^{-/-}$ arteries respectively (Fig. 2.A, Supplemental Table 1.A). From this screen, 175 differential proteins were identified based on the threshold of $p < 0.05$ (Fig. 2.B). Of these, 91 proteins showed increased abundance in Col8$^{-/-}$ vessels, including VSMC markers (Acta2, Smtn, Cnn1), elastic (Eln, Lox, Emilin 1) and non-fibrillar collagen proteins (Col4a3, Col6a1, Col14a1, Col15a1, Col18a1), which are highlighted in the volcano plot (Fig. 2.C, Supplemental Table 1.B). 85 proteins showed decreased abundance in Col8$^{-/-}$ vessels, including the most significant hits (Glrx3, Anxa5, Anxa1), and those with the biggest fold changes including Dapk3 and Dsp. GO pathway analysis identifies important functions for these proteins in the regulation of actin organization, cell motility and junction formation. To further quantify changes in matrix composition, biochemical assays were utilized to measure crosslinked elastin (desmosine) and collagen (hydroxyproline) content in Col8$^{+/+}$ and Col8$^{-/-}$ vessels. Elastin content was significantly increased in Col8$^{-/-}$ carotid arteries relative to wildtype (Fig. 2.D), whereas collagen content was comparable between groups (Fig. 2.E). Analyses to measure elastin and collagen content through histological staining were also performed (Supplemental Fig. 3 however no significant differences were determined, possibly due to the reduced sensitivity of this technique relative to the biochemical assays presented in Fig. 2.

Phenylephrine-induced phosphorylation of MYPT1 was enhanced in Col8$^{-/-}$ VSMCs, and smooth muscle cell marker expression was increased

We hypothesized that the increase in PE-induced contractility (Fig. 1.G) was due to activation of actomyosin, and immunoblotted for myosin phosphatase target subunit 1 (MYPT1). MYPT1 dephosphorylates myosin light chain (MLC), which stops cross bridge formation. However, when MYPT1 is phosphorylated, it cannot perform its phosphatase function, enabling persistent cell contraction. We measured total and phosphorylated levels of MYPT1 protein as a surrogate of cell contractility in Col8$^{+/+}$ and Col8$^{-/-}$ cells stimulated with PE. We determined that the phosphorylated to total MYPT1 ratio was increased 2-fold in the Col8$^{-/-}$ cells (Fig. 3.A-B). Moreover, since Col8$^{-/-}$ arteries demonstrated enhanced PE-induced contractility and upregulated VSMC marker proteins in the proteomic screen, we hypothesized that VSMC marker expression would also be increased and performed immunoblotting in Col-8$^{+/+}$ and Col8$^{-/-}$ cells to confirm this. After 12 days in culture, expression levels of αSMA, SM22 and calponin were enhanced in the Col8$^{-/-}$ VSMCs (Fig. 3.C-F), which substantiate the mass spectrometry results (Fig. 2.C), but we observed no change in SM-MHC (Fig. 3G.

Differential matrix composition in Col8$^{+/+}$ and Col8$^{-/-}$ VSMCs in vitro

To test our hypothesis that Col-8 functions in the regulation of matrix to maintain vessel integrity, we performed *in vitro* studies to evaluate the synthesis and deposition of selected ECM proteins: elastic fibers, collagen fibers and fibronectin. Elastic and collagen fibers are the dominant load bearing proteins in the vessel wall, while fibronectin is a key matrix protein necessary for the assembly of both collagens and elastin into functional fibers. Synthesis and assembly of these matrix proteins was assessed in Col8$^{+/+}$ and Col8$^{-/-}$ VSMCs cultured for 12 days.

There was a 53-fold increase in tropoelastin mRNA level in Col8$^{-/-}$ VSMCs compared to Col8$^{+/+}$ cells (Fig. 4.A). The mRNA levels for *Fbn2*, *Fbln5*, *Emilin1* and *Magp1* were also increased in Col8$^{-/-}$ compared to Col8$^{+/+}$ cells. The expression of *Col3a1* was reduced by 13-fold in Col8$^{-/-}$ relative to Col8$^{+/+}$ VSMCs (Fig. 4.B), with no significant differences in *Col1a1*, *Col1a2*, *Col5a1*, *Col5a2*, or *Col5a3*. Next, to determine whether Col-8 functions in matrix deposition, we studied the ECM proteins: elastin, collagen-I, and fibronectin. Col8$^{+/+}$ and Col8$^{-/-}$ cells were cultured for 12 days, followed by decellularization and immunostaining of the cell derived ECM. There was significant deposition of elastic fibers in Col8$^{-/-}$ cell cultures, with almost no elastic fibers present in Col8$^{+/+}$ cell cultures (Fig. 4.C). Collagen-I fibers were reduced in the Col8$^{-/-}$ cells, while there was little change in fibronectin deposition (Fig. 4.C). Measurement of mean fluorescence intensity confirmed the robust accumulation of elastic fibers in the matrix from Col8$^{-/-}$ cells which was dramatically attenuated in the Col8$^{+/+}$ matrix (Fig. 4.D). Collagen-I deposition was reduced in Col8$^{-/-}$ cells relative to Col8$^{+/+}$ (Fig. 4.E). There was no significant difference in fibronectin deposition between the two cell types (Fig. 4.F).

Exogenous rCol-8 reduced tropoelastin mRNA levels and elastic fiber deposition in Col8$^{-/-}$ VSMCs in vitro

To determine whether the defects in elastin synthesis and assembly in the Col8$^{-/-}$ cells

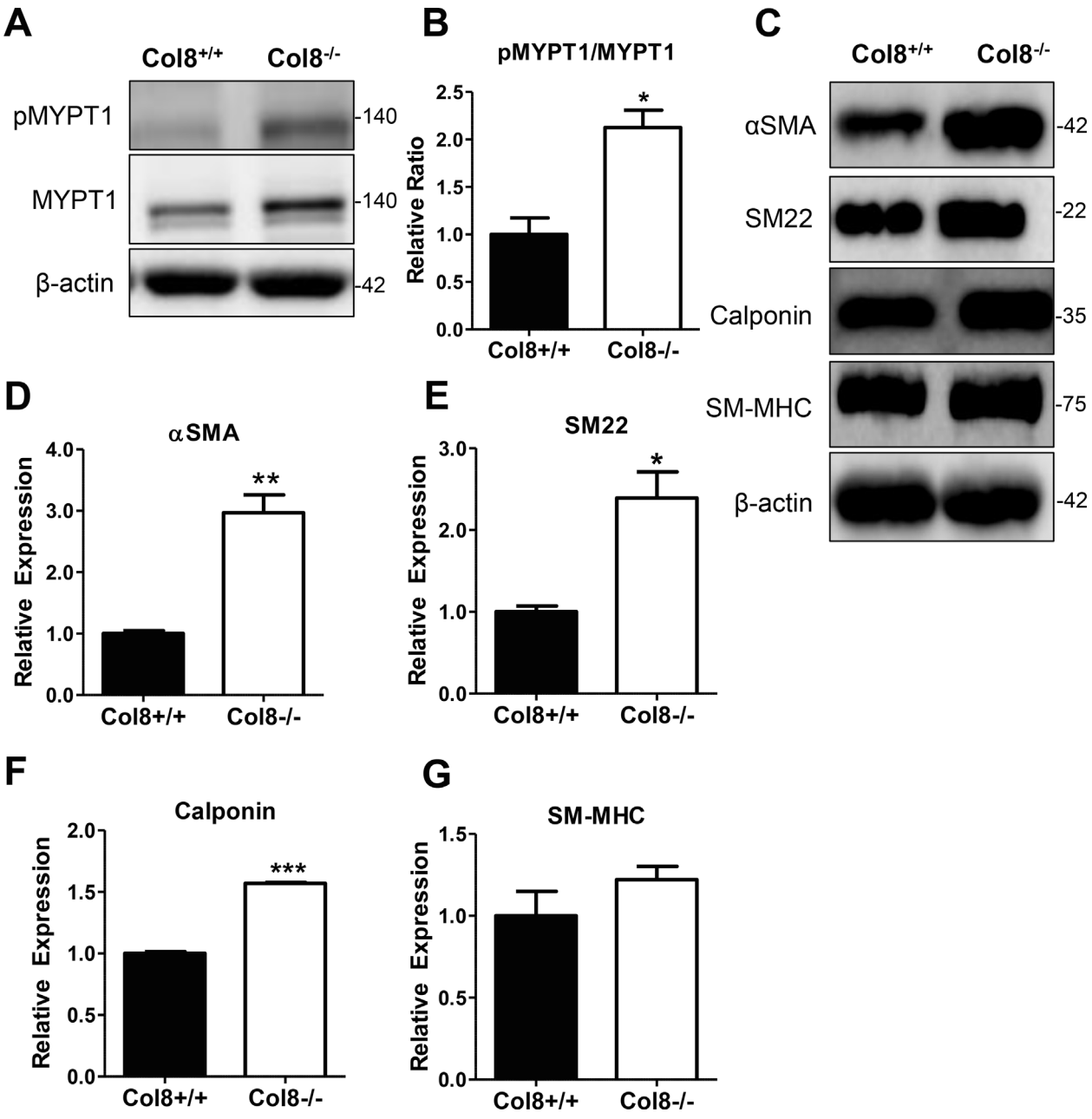

Fig. 3. Phenylephrine-induced phosphorylation of MYPT1 was enhanced in Col8$^{-/-}$ VSMCs, and smooth muscle cell marker expression was increased. A-B, serum starved Col8$^{+/+}$ and Col8$^{-/-}$ VSMCs were stimulated with 10 μM PE for 10 min and immunoblotted for pMYPTI/MYPT1. **C**, Col8$^{+/+}$ and Col8$^{-/-}$ VSMCs were immunoblotted for VMSC markers. Quantification for αSMA (**D**); SM22 (**E**); Calponin (**F**); SM-MHC (**G**) is depicted. All band intensities were normalized to β-actin. Values represent the mean ± SEM (n = 3), *p < 0.05; **p < 0.01; ***p < 0.001.

could be rescued, we cultured cells on exogenously synthesized recombinant Col-8 protein (rCol-8). Exogenous rCol-8 (+VIII) diminished the elastic fiber deposition observed in Col8$^{-/-}$ cells (Fig. 5.A-B). The Col8$^{-/-}$ cells treated with rCol-8 still deposited elastic fibers, but the density was much lower and the staining intensity of the fibers reduced. Furthermore, treatment of Col8$^{-/-}$ cells with rCol-8 dramatically limited tropoelastin mRNA expression such that it was not significantly different compared to Col8$^{+/+}$ cells (Fig. 5.C). This was in sharp contrast to the significant 53-fold increase that was observed without the exogenous Col-8 (Fig. 4.A).

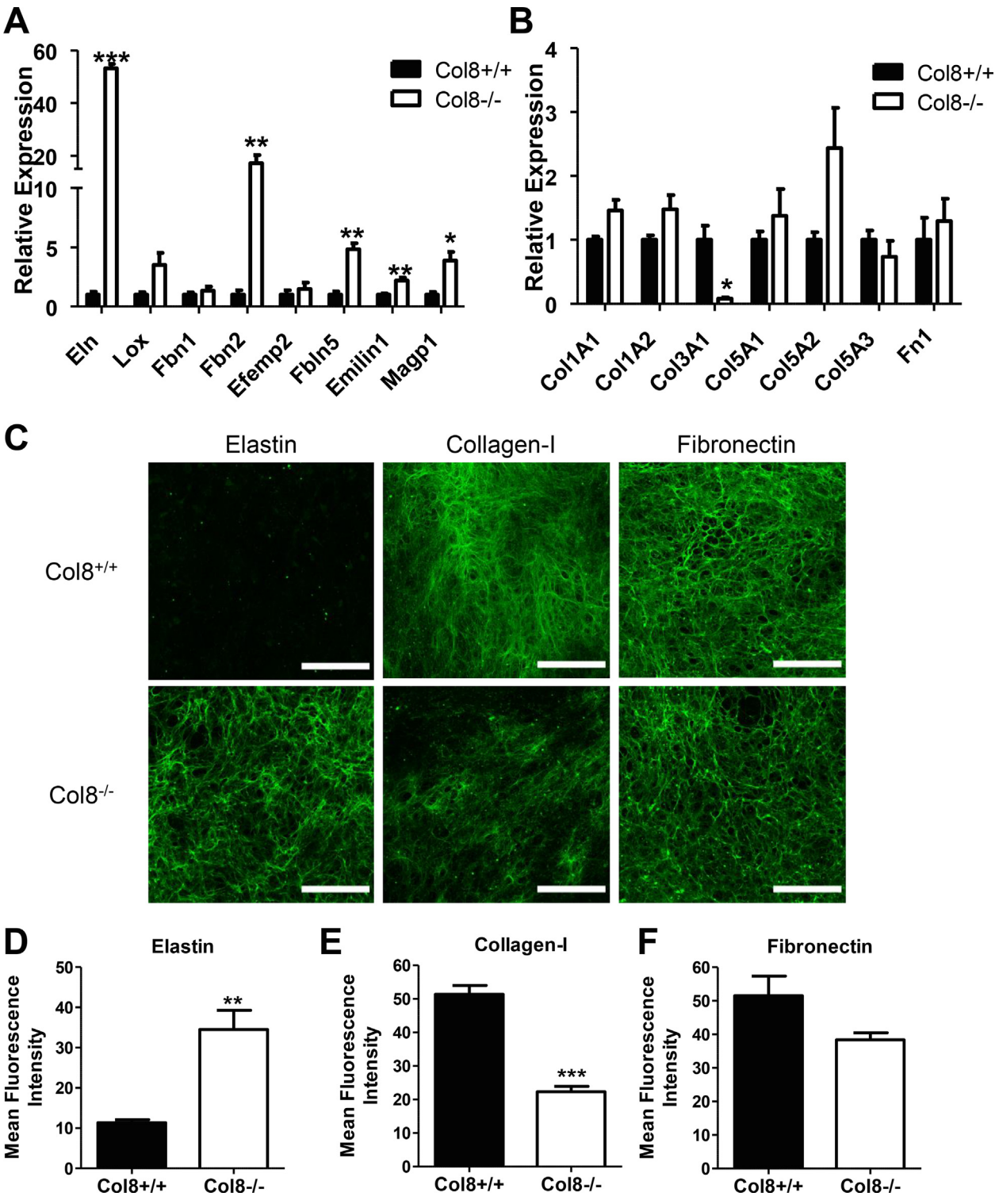

Fig. 4. Differential matrix composition in Col8$^{+/+}$ and Col8$^{-/-}$ VSMCs *in vitro*. A-B, Expression levels for ECM genes related to elastic fiber proteins (Eln, Lox, Fbn1, Fbn2, Efemp2, Fbln5, Emilin1, Magp1), collagens (Col1a1, Col1a2, Col3a1, Col5a1, Col5a2, Col5a3), and fibronectin were determined by qRT-PCR. **C**, Decellularized matrices were labeled for either elastin, fibronectin or collagen-I. Scale bar = 100 μM. Mean intensity quantified for **D**, elastin (green); **E**, collagen-I (green); **F**, fibronectin (green). Values represent the mean ± SEM (n = 3), *p < 0.05; **p < 0.01, ***p < 0.001. (For interpretation of the references to colour in this figure legend, the reader is referred to the web version of this article.)

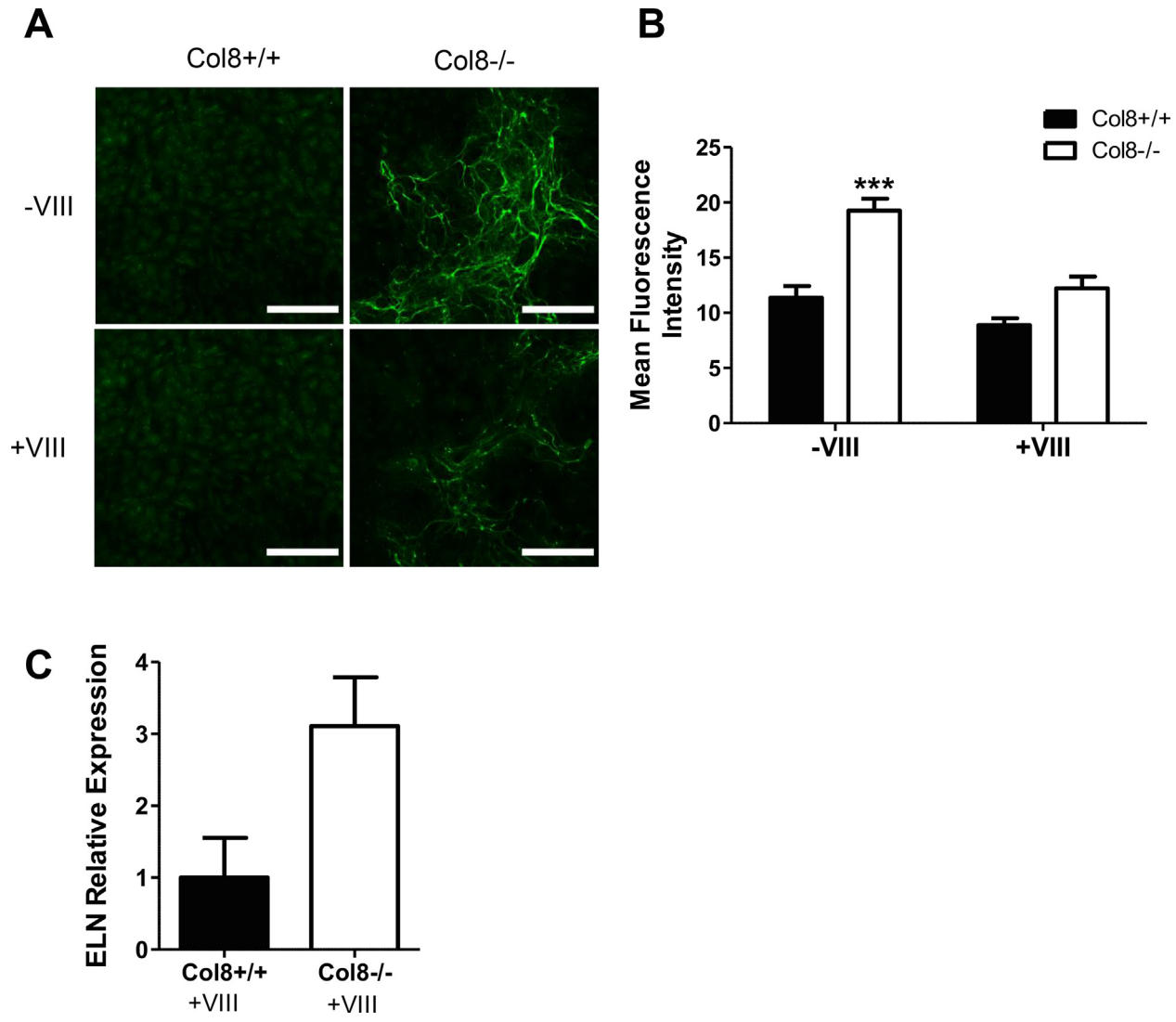

Fig. 5. Exogenous rCol-8 reduced tropoelastin mRNA levels and elastic fiber deposition in Col8$^{-/-}$ VSMCs *in vitro*. **A-B**, Col8$^{+/+}$ and Col8$^{-/-}$ VSMCs were cultured in the presence or absence of 2 μg/cm^2 exogenous collagen VIII coated on the plates (-/+ VIII). Cells were labeled for elastin (green) and mean intensity quantified. Scale bar = 100 μM. **C**, mRNA was isolated from Col8$^{+/+}$ and Col8$^{-/-}$ VSMCs cultured in the presence of exogenous collagen VIII (+VIII) and *Eln* expression levels were determined by qRT-PCR. Values represent the mean ± SEM (n = 3), ***p < 0.001. (For interpretation of the references to colour in this figure legend, the reader is referred to the web version of this article.)

Discussion

The purpose of our study was to determine whether Col-8 is important for the maintenance of elastic vessel integrity. Using Col8$^{+/+}$ and Col8$^{-/-}$ mice we demonstrated that Col8$^{-/-}$ mice have an arterial system that is more compliant, evidenced by reduced MAP, and increased vessel distensibility, indicating an enhanced Windkessel effect. Differences in both the matrix composition and VSMC function resulted in Col8$^{-/-}$ carotid arteries that displayed increased diameters under pressure-induced stretching, but enhanced catecholamine-induced contractility – which may compensate for sustained resilience to pressure. Moreover, in VSMCs cultured *in vitro*, the absence of Col-8 dramatically increased tropoelastin mRNA expression and elastic fiber deposition in the ECM, which was attenuated upon treatment with exogenous rCol-8 protein. We therefore report for the first time a causative role for Col-8 in reducing mRNA levels of tropoelastin and subsequently limiting the deposition of elastic fibers in the extracellular matrix.

Here we demonstrate through *in vivo* studies that in carotid arteries from adult mice, the absence of Col-8 increased vessel compliance and elastin deposition. The measurement of functional

distensibility (FD) revealed that the Col8$^{-/-}$ vessels achieved the same outer diameter as wildtype, but required lower distending pressure to accomplish this, hence indicating a more compliant carotid artery. Both collagen and elastic fibers work in unison to regulate the mechanical properties of the conduit vessel. Collagen-I and collagen-III are the dominant fibrillar collagens in the vessel wall and confer tensile strength while preventing over distension of the tissue. Using *in vitro* studies, we found a reduction in the mRNA expression of *Col3a1* and deposition of collagen-I in our Col8$^{-/-}$ VSMCs, suggesting a role for Col-8 in regulating the remodeling of collagens. These findings extend previous reports on the role of Col-8 during matrix remodeling processes. Col-8 functions as a provisional matrix protein: it is deposited as a primary step during tissue remodeling and it is degraded once a more permanent ECM rich in fibrillar collagens has been synthesized [32]. Furthermore, previous studies have shown reduced fibrillar collagen synthesis and assembly [33], and reduced fibrillar collagen organization [9] in the absence of Col-8. Disruptions in collagen synthesis and assembly could impact upon vessel distensibility, especially in vessels operating at high pressures, however, since fibrillar collagen engagement is minimal at normal physiological pressures [31], the increased distensibility in the Col8$^{-/-}$ arteries is more likely due to changes in the elastic fibers. Elastic fibers are the dominant ECM vessel wall protein and confer extensibility to the artery – directly impacting its compliance. The increased compliance in the Col8$^{-/-}$ arteries led us to hypothesize that these vessels would have increased elastic fibers. In agreement, Col8$^{-/-}$ carotid arteries had increased elastin protein in the proteomic screen, and greater crosslinked elastin content measured via biochemical assays of desmosine content, compared to wildtype arteries.

We have uncovered a reciprocal relationship between Col-8 and elastin synthesis in VSMCs. After long term tissue culture, there was a dramatic 53-fold increase in tropoelastin mRNA in the Col8$^{-/-}$ VSMCs compared to Col8$^{+/+}$ cells, which was accompanied by the robust deposition of elastic fibers in the ECM of the Col8$^{-/-}$ VSMCs. Furthermore, when Col8$^{-/-}$ cells were cultured with exogenous rCol-8 protein, it abolished the increase in tropoelastin mRNA and significantly limited the deposition of elastic fibers in the ECM to only a 3-fold increase. Therefore, there was a 94% reduction in tropoelastin expression in the knockout cells due to exogenous Col8 treatment. To our knowledge, this is the first demonstration that Col-8 negatively regulates the mRNA levels of tropoelastin and the formation of elastic fibers by VSMCs. This proposed model is summarized in Fig. 6. The synthesis of elastic fibers begins with transcription of the tropoelastin gene and then translation of the transcript into elastin monomers. These monomers are secreted out of the cell and organized onto the microfibril scaffold to form functional elastic fibers. Col-8 is present in the ECM, and signals into the cell (possibly through $\alpha_2\beta_1$ integrins [32]) to reduce the levels of tropoelastin mRNA. This reduction of transcript therefore limits monomer production and the synthesis of mature elastic fibers. The specific signaling pathway involved in the regulation of tropoelastin by Col-8 remains to be defined, and will be the focus of future work.

Previous reports using microarray gene expression profiling in the developing mouse aorta showed that the temporal expression of Col-8 and elastin is different [34]. Procollagen type VIII, alpha 1 (*Col8a1*) expression was upregulated during embryogenesis (like fibrillins and LOX), whereas elastin expression was low in the embryo, but increased in the postnatal stages. Based on this pattern of expression, we suggest that Col-8 signaling may repress *Eln* expression during embryogenesis, which is reversed as levels of Col-8 decrease postnatally. This would explain why there is a robust accumulation of tropoelastin and elastic fibers in the Col8$^{-/-}$ cells *in vitro*, and a subsequent increase in vessel compliance *ex vivo* in Col8$^{-/-}$ mice. In the vasculature, downregulation of Col-8 post embryonic development may enable Col8$^{+/+}$ mice to accumulate elastin and assemble elastic fibers to develop a functional vascular system. Apart from our focus on Col-8 and elastin, other ECM proteins such as proteoglycans have also been identified to impact elastic fiber synthesis and assembly. Expression of the V3 variant of versican has been associated with increased synthesis and deposition of elastin by VSMCs and fibroblasts [35,36]. Furthermore overexpression of V3 stimulates myocardin to maintain VSMCs in the differentiated phenotype, [37], suggesting an opposing action to that of Col-8. Hyaluronan also stimulates elastin synthesis by VSMCs, which has been utilized to improve elastin content in engineered vascular grafts [38–40]. Heparan sulfate proteoglycans regulate microfibril assembly and deposition of elastin onto the scaffold [41]. Furthermore, there is a reduction in tropoelastin synthesis in the presence of excess chondroitin sulfate proteoglycans [42]. Collectively these findings indicate the complexity of elastogenesis and identify an area for continued investigation.

Another major finding of our report is that there are opposing effects of Col-8 and elastin on VSMC phenotype which we confirmed through *in vivo* and *in vitro* studies: Col-8 elicits a synthetic phenotype, while elastin confers quiescence. In the adult carotid artery, VSMCs exist in a quiescent and contractile phenotype. Maintenance of this state is imposed in part through tropoelastin signaling and the presence of intact elastic lamellae, which limit cell migration and proliferation, and promote maturation [43]. Elastin promotes RhoA activity which controls the

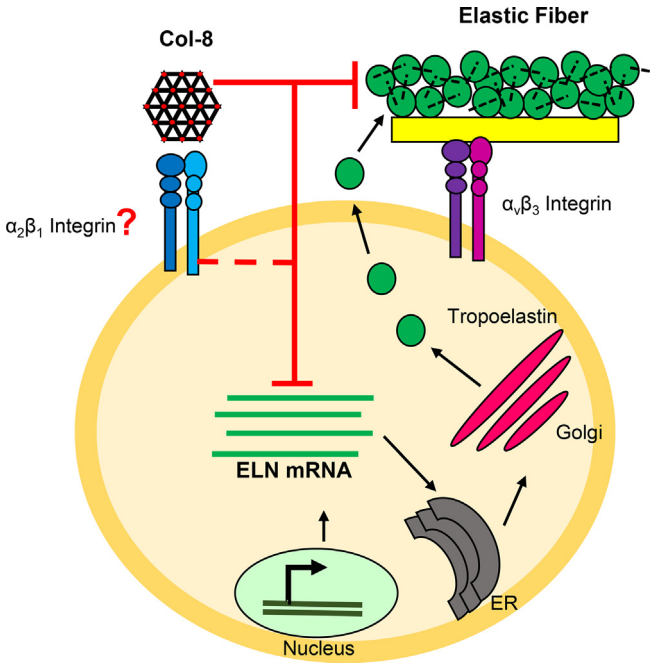

Fig. 6. Working hypothesis model of Col-8 inhibiting elastin. The transcription, translation and formation of tropoelastin into elastic fibers is depicted by black arrows. Col-8 reduced tropoelastin mRNA levels and elastic fibers, as depicted by red inhibiting lines. Col-8 is hypothesized to perform these functions through $\alpha_2\beta_1$ integrin signaling, which is outlined as a hashed red inhibiting line. (For interpretation of the references to colour in this figure legend, the reader is referred to the web version of this article.)

expression of VSMC specific genes like *Acta2*, *Cnnl*, *Tagln*, and *Myh11*, via serum response factor (SRF) [44,45]. By contrast, disruptions to arterial wall homeostasis such as vessel injury and atherosclerosis trigger VSMC transition to the active and synthetic cell phenotype [46]. Col-8 inhibits RhoA activity [10], promotes VSMC proliferation [47,48], acts as a chemotactic factor for both medial and intimal VSMCs [32], and as a provisional matrix to facilitate haptotactic responses during migration [48,49]. Thus Col8$^{-/-}$ VSMCs show decreased proliferation, migration and elevated RhoA activity which are all hallmark features of the quiescent contractile VSMC. There are other pathways by which Col-8 may influence VSMC phenotype, for example previous studies have shown that Col-8 expression is correlated with downregulation of KLF-4, which occurs during the transition of VSMCs from a quiescent to active phenotype following vascular injury [50]. However, no studies to date have directly addressed the signaling involved. It is also possible that Col-8 influences VSMC phenotype directly by modulating integrin dependent RhoA activation, leading to modulation of MRTF-A which controls VSMC phenotype [51].

Here, we showed that VSMCs in Col8$^{-/-}$ carotid arteries were of the contractile phenotype. The proteomic screen revealed the upregulation of VSMC maturation markers in Col8$^{-/-}$ vessels and they displayed enhanced responsiveness to PE induced vasoconstriction. We showed *in vitro* that the absence of Col-8 increased expression of αSMA, SM22 and calponin, and activity of the contractile apparatus protein MYPT1. Though this observation may seem at odds with increased distensibility of the Col8$^{-/-}$ vessels, it is important to note that VSMCs in elastic vessels have very little contractile activity compared to those composing resistance arteries [52]. Therefore, the increase in PE responsiveness that we observed likely compensates for reduced vessel integrity and structural support in the absence of Col-8. Despite the cells being more responsive to a vasoconstrictor, we have not measured the amounts of circulating catecholamine levels in Col8$^{+/+}$ and Col8$^{-/-}$ mice to know if this mechanism is actively engaged. Furthermore, the increase in VSMC markers coincide with a more mature VSMC, which is in agreement with the increases in elastin synthesis observed, and the mechanistic coupling between these two phenotypic characteristics [43].

We suggest that the quiescent-like phenotype adapted by Col8$^{-/-}$ VSMCs *in vitro* recapitulates their *in vivo* environment. In culture, VSMCs deficient in Col-8 deposited a distinctly dense matrix rich in elastic fibers (mimicking elastic lamellae), which could trigger VSMC contractile marker expression and activity s. These findings directly relate to the regulatory role of Col-8 on tropoelastin mRNA levels, and further strengthen our hypothesis that in the absence of Col-8, elastin is upregulated, accumulates in the ECM, and signals to promote VSMC maturation. In agreement, Karnik *et al.* [43] reported that VSMCs

deficient in elastin ($Eln^{-/-}$) have reduced VSMC marker expression, but enhanced proliferative and migratory capacity, resulting in vessel stenosis in $Eln^{-/-}$ mice, similar to our $Col8^{+/+}$ VSMCs. $Eln^{-/-}$ mice also have *Col8a1* as their most upregulated transcript [15], suggesting that Col-8 contributes to the synthetic and hyper-proliferative phenotype of those VSMCs.

Our studies were focused on conduit arteries, where Col-8 expression has been detected during development and was markedly upregulated in vascular disease. Though the microvasculature is a master regulator of blood pressure, the expression and function of Col-8 in resistance arteries has not been studied. However, due to the dominant role RhoA plays in contributing to arteriolar tone, and the inhibitory effect Col-8 has on RhoA [10], it is not likely that Col-8 is a persistent matrix protein in these vessels. Future studies related to understanding the inverse relationship between Col-8 and elastin should focus on whether elastin regulates Col-8 expression. It is plausible that a negative feedback relationship between elastin and Col-8 exists, such that the expression of the former turns off the latter. The expression timeline of these proteins are consistent with this hypothesis [34]. Elastin-mediated regulation of Col-8 expression would also explain why *Col8a1* is the most upregulated transcript in $Eln^{-/-}$ mice [15]. Moreover, since the pattern of expression of Col-8 can be described as fetal gene reprogramming during disease, the loss of intact elastic fibers and tropoelastin signaling may be a mechanistic cue to turn on Col-8 expression.

We have demonstrated that Col-8 deficiency leads to increased elastin content and compliance in arteries. These findings could point to an approach to synthesize and assemble elastic fibers, a process which is developmentally restricted [52]. Therapeutics aimed at improving the elastin content of vessels are needed, particularly for patients suffering the adverse effects of arterial stiffening, or those with genetic elastinopathies [53]. Previous attempts to restore elastin in vessels, have resulted in functional improvements. For example, introducing the human elastin gene with a bacterial artificial chromosome into elastin haploinsufficient ($Eln^{+/-}$) mice caused elastin levels to increase by 20% in the vessel wall, and improved compliance to levels similar to that seen in wildtype vessels [31,54]. Other groups have investigated methods to increase elastin or improve compliance in $Eln^{+/-}$ mice through chemical intervention such as microRNA inhibitors. Zhang *et al.* [55] identified that inhibition of miR29a could selectively upregulate *Eln* mRNA levels in human VSMCs and dermal fibroblasts from patients with elastin insufficiencies, and this improved the compliance of human bioengineered vessels at low pressures. There is considerable interest in using V3 versican and hyaluronan to increase the elastin content of engineered skin and vascular grafts [56–58]. Taken together, these studies demonstrate the direct benefit of reversing stiffness by increasing elastin content. Here, we propose a new mechanism to improve the elastin content and compliance of vessels – deletion or inhibition of Col-8. Thus, future studies regarding the potential of Col-8 in matrix biology are not only exciting, but essential.

CRediT authorship contribution statement

Amanda L. Mohabeer: Conceptualization, Methodology, Formal analysis, Investigation, Writing – original draft, Visualization. **Jeffrey T. Kroetsch:** Conceptualization, Methodology, Resources, Writing – review & editing. **Meghan McFadden:** Methodology, Validation, Formal analysis, Investigation, Data curation, Writing – review & editing, Visualization. **Negin Khosraviani:** Investigation, Writing – review & editing. **Thomas J. Broekelmann:** Formal analysis, Investigation. **Guangpei Hou:** Resources, Investigation. **Hangjun Zhang:** Investigation. **Yu-Qing Zhou:** Investigation, Formal analysis, Writing – review & editing. **Minyao Wang:** Investigation. **Anthony O. Gramolini:** Resources, Supervision. **Robert P. Mecham:** Validation, Resources, Writing – review & editing, Supervision. **Scott P. Heximer:** Supervision, Conceptualization, Writing – review & editing. **Steffen-Sebastian Bolz:** Conceptualization, Resources, Supervision. **Michelle P. Bendeck:** Conceptualization, Validation, Writing – review & editing, Supervision, Project administration, Funding acquisition.

DECLARATION OF COMPETING INTEREST

The authors declare that they have no known competing financial interests or personal relationships that could have appeared to influence the work reported in this paper.

Acknowledgements

We would like to thank Dr. Richard Assoian (University of Pennsylvania) for his advice and support with the development of this study. We would also like to thank Dr. Jessica Wagenseil (Washington University) and her lab for their generous help with pressure myography training. Lastly, thank you to Laura-lee Caruso for maintenance of the mouse colonies.

This work was supported by grants from the Canadian Institutes of Health Research

(MOP126042) and the National Institutes of Health (HL110346) to MPB.

Appendix A. Supplementary data

Supplementary data to this article can be found online at https://doi.org/10.1016/j.mbplus.2021.100085.

Received 17 June 2021;
Accepted 21 September 2021;
Available online 29 September 2021

Keywords:
Fibrosis;
Collagen;
Fibrillogenesis;
Proteolysis;
Therapeutic target;
Biomarker

† Present address: Helmholtz Institute for pharmaceutical sciences Campus E8 1, 66123 Saarbrücken, Germany.

Abbreviations:
ADAMTS, a disintegrin and metalloproteinase with thrombospondin motifs; AS, aortic valve stenosis; BMP, bone morphogenetic protein; CVD, cardiovascular disease; CKD, chronic kidney disease; CP, C-propeptide; CUB, complement, Uegf, BMP-1; DMD, Duchenne muscular dystrophy; ECM, extracellular matrix; EGF, epidermal growth factor; eGFR, estimated glomerular filtration rate; ELISA, enzyme-linked immunosorbent assay; HDL, high-density lipoprotein; HSC, hepatic stellate cell; HTS, hypertrophic scar; IPF, idiopathic pulmonary fibrosis; LDL, low-density lipoprotein; MI, myocardial infarction; MMP, matrix metalloproteinase; mTLD, mammalian tolloid; mTLL, mammalian tolloid-like; NASH, nonalcoholic steatohepatitis; NTR, netrin; PABPN1, poly(A)-binding protein nuclear 1; OPMD, oculopharyngeal muscular dystrophy; PCP, procollagen C-proteinase; PCPE, procollagen C-proteinase enhancer; PNP, procollagen N-proteinase; SPC, subtilisin proprotein convertase; TIMP, tissue inhibitor of metalloproteinases; TGF-β, transforming growth-factor β; TSPN, thrombospondin-like N-terminal

References

[1] Mitchell, G.F., Hwang, S.-J., Vasan, R.S., Larson, M.G., Pencina, M.J., Hamburg, N.M., Vita, J.A., Levy, D., Benjamin, E.J., (2010). Arterial stiffness and cardiovascular events: the Framingham Heart Study. *Circulation*, **121** (4), 505–511.

[2] Dobrin, P.B., (1978). Mechanical properties of arteries. *Physiol. Rev.*, **58** (2), 397–460.

[3] Stephan, S., Sherratt, M.J., Hodson, N., Shuttleworth, C. A., Kielty, C.M., (2004). Expression and supramolecular assembly of recombinant alpha1(viii) and alpha2(viii) collagen homotrimers. *J. Biol. Chem.*, **279** (20), 21469–21477.

[4] Sage, H., Balian, G., Vogel, A.M., Bornstein, P., (1984). Type VIII collagen. Synthesis by normal and malignant cells in culture. *Lab. Invest.*, **50** (2), 219–231.

[5] Ricard-Blum, S., Dublet, B., Van, R.M., (2000). Unconventional collagens: Types VI, VII, VIII, IX, X, XII, XIV, XVI, and XIX. Oxford University Press, Oxford.

[6] Dapena, I., Ham, L., Droutsas, K., van Dijk, K., Moutsouris, K., Melles, G.R.J., (2011). Learning Curve in Descemet's Membrane Endothelial Keratoplasty: First Series of 135 Consecutive Cases. *Ophthalmology*, **118** (11), 2147–2154.

[7] Tamura, Y., Konomi, H., Sawada, H., Takashima, S., Nakajima, A., (1991). Tissue distribution of type VIII collagen in human adult and fetal eyes. *Invest. Ophthalmol. Vis. Sci.*, **32** (9), 2636–2644.

[8] MacBeath, J.R., Kielty, C.M., Shuttleworth, C.A., (1996). Type VIII collagen is a product of vascular smooth-muscle cells in development and disease. *Biochem. J.*, **319** (Pt 3), 993–998.

[9] Lopes, J., Adiguzel, E., Gu, S., Liu, S.-L., Hou, G., Heximer, S., Assoian, R.K., Bendeck, M.P., (2013). Type VIII collagen mediates vessel wall remodeling after arterial injury and fibrous cap formation in atherosclerosis. *Am. J. Pathol.*, **182** (6), 2241–2253.

[10] Adiguzel, E., Hou, G., Sabatini, P.J., Bendeck, M.P., (2013). Type VIII collagen signals via beta1 integrin and RhoA to regulate MMP-2 expression and smooth muscle cell migration. *Matrix Biol.*, **32** (6), 332–341.

[11] Qiu, H., Depre, C., Ghosh, K., Resuello, R.G., Natividad, F.F., Rossi, F., Peppas, A., Shen, Y.-T., Vatner, D.E., Vatner, S.F., (2007). Mechanism of gender-specific differences in aortic stiffness with aging in nonhuman primates. *Circulation*, **116** (6), 669–676.

[12] Plenz, G., Dorszewski, A., Breithardt, G., Robenek, H., (1999). Expression of type VIII collagen after cholesterol diet and injury in the rabbit model of atherosclerosis. *Arterioscler. Thromb. Vasc. Biol.*, **19** (5), 1201–1209.

[13] Hinton, R.B., Adelman-Brown, J., Witt, S., Krishnamurthy, V.K., Osinska, H., Sakthivel, B., James, J.F., Li, D.Y., Narmoneva, D.A., Mecham, R.P., Benson, D.W., (2010). Elastin haploinsufficiency results in progressive aortic valve malformation and latent valve disease in a mouse model. *Circ. Res.*, **107** (4), 549–557.

[14] Kielty, C.M., Sherratt, M.J., Shuttleworth, C.A., (2002). Elastic fibres. *J. Cell Sci.*, **115** (Pt 14), 2817–2828.

[15] Staiculescu, M.C., Cocciolone, A.J., Procknow, J.D., Kim, J., Wagenseil, J.E., (2018). Comparative gene array analyses of severe elastic fiber defects in late embryonic and newborn mouse aorta. *Physiol. Genomics*, **50** (11), 988–1001.

[16] Hopfer, U., Fukai, N., Hopfer, H., Wolf, G., Joyce, N., Li, E. n., Olsen, B.R., (2005). Targeted disruption of Col8a1 and Col8a2 genes in mice leads to anterior segment abnormalities in the eye. *FASEB J.*, **19** (10), 1232–1244.

[17] Noyan-Ashraf, M.H., Momen, M.A., Ban, K., Sadi, A.-M., Zhou, Y.-Q., Riazi, A.M., Baggio, L.L., Henkelman, R.M., Husain, M., Drucker, D.J., (2009). GLP-1R agonist liraglutide activates cytoprotective pathways and improves outcomes after experimental myocardial infarction in mice. *Diabetes*, **58** (4), 975–983.

[18] Amin, M., Le, V.P., Wagenseil, J.E., (2012). Mechanical testing of mouse carotid arteries: from newborn to adult. *J. Vis. Exp.*, **60**

[19] Sinha, A., Ignatchenko, V., Ignatchenko, A., Mejia-Guerrero, S., Kislinger, T., (2014). In-depth proteomic analyses of ovarian cancer cell line exosomes reveals differential enrichment of functional categories compared to the NCI 60 proteome. *Biochem. Biophys. Res. Commun.*, **445** (4), 694–701.

[20] Cox, J., Hein, M.Y., Luber, C.A., Paron, I., Nagaraj, N., Mann, M., (2014). Accurate proteome-wide label-free quantification by delayed normalization and maximal peptide ratio extraction, termed MaxLFQ. *Mol. Cell. Proteomics*, **13** (9), 2513–2526.

[21] Stoilov, I., Starcher, B.C., Mecham, R.P., Broekelmann, T. J., (2018). Measurement of elastin, collagen, and total protein levels in tissues. *Methods Cell Biol.*, **143**, 133–146.

[22] Hou, G., Vogel, W., Bendeck, M.P., (2001). The discoidin domain receptor tyrosine kinase DDR1 in arterial wound repair. *J. Clin. Invest.*, **107** (6), 727–735.

[23] Kothapalli, D., Liu, S.-L., Bae, Y., Monslow, J., Xu, T., Hawthorne, E., Byfield, F., Castagnino, P., Rao, S., Rader, D., Puré, E., Phillips, M., Lund-Katz, S., Janmey, P., Assoian, R., (2012). Cardiovascular protection by ApoE and ApoE-HDL linked to suppression of ECM gene expression and arterial stiffening. *Cell Rep.*, **2** (5), 1259–1271.

[24] Makihara, H., Hidaka, M., Sakai, Y., Horie, Y., Mitsui, H., Ohashi, K., Goshima, Y., Akase, T., (2017). Reduction and fragmentation of elastic fibers in the skin of obese mice is associated with altered mRNA expression levels of fibrillin-1 and neprilysin. *Connect. Tissue Res.*, **58** (5), 479–486.

[25] Braghetta, P., Ferrari, A., de Gemmis, P., Zanetti, M., Volpin, D., Bonaldo, P., Bressan, G.M., (2002). Expression of the EMILIN-1 gene during mouse development. *Matrix Biol.*, **21** (7), 603–609.

[26] Tatano, Y., Shimizu, T., Tomioka, H., (2014). Unique macrophages different from M1/M2 macrophages inhibit T cell mitogenesis while upregulating Th17 polarization. *Sci. Rep.*, **4**, 4146.

[27] Fujikawa, Y., Yoshida, H., Inoue, T., Ohbayashi, T., Noda, K., von Melchner, H., et al., (2017). Latent TGF-beta binding protein 2 and 4 have essential overlapping functions in microfibril development. *Sci. Rep.*, **7**, 43714.

[28] Choi, J., Bergdahl, A., Zheng, Q., Starcher, B., Yanagisawa, H., Davis, E.C., (2009). Analysis of dermal elastic fibers in the absence of fibulin-5 reveals potential roles for fibulin-5 in elastic fiber assembly. *Matrix Biol.*, **28** (4), 211–220.

[29] Schmittgen, T.D., Livak, K.J., (2008). Analyzing real-time PCR data by the comparative C(T) method. *Nat. Protoc.*, **3** (6), 1101–1108.

[30] Fisher, M., Jones, R.A., Huang, L., Haylor, J.L., El Nahas, M., Griffin, M., Johnson, T.S., (2009). Modulation of tissue transglutaminase in tubular epithelial cells alters extracellular matrix levels: a potential mechanism of tissue scarring. *Matrix Biol.*, **28** (1), 20–31.

[31] Wagenseil, J.E., Mecham, R.P., (2012). Elastin in large artery stiffness and hypertension. *J. Cardiovasc. Transl. Res.*, **5** (3), 264–273.

[32] Hou, G., Mulholland, D., Gronska, M.A., Bendeck, M.P., (2000). Type VIII Collagen Stimulates Smooth Muscle Cell Migration and Matrix Metalloproteinase Synthesis after Arterial Injury. *Am. J. Pathol.*, **156** (2), 467–476.

[33] B. Skrbic, K.V. Engebretsen, M.E. Strand, I.G. Lunde, K. M. Herum, H.S. Marstein, et al. Lack of collagen VIII reduces fibrosis and promotes early mortality and cardiac dilatation in pressure overload in mice. Cardiovasc Res. 2015;106(1):32-42.

[34] S.E. McLean, B.H. Mecham, C.M. Kelleher, T.J. Mariani, R.P. Mecham, Extracellular matrix gene expression in the developing mouse aorta Extracellular Matrix in Development and Disease, Adv. Dev. Biol., 2005, 81-128.

[35] Merrilees, M.J., Beaumont, B.W., Braun, K.R., Thomas, A. C., Kang, I., Hinek, A., Passi, A., Wight, T.N., (2011). Neointima formed by arterial smooth muscle cells expressing versican variant V3 is resistant to lipid and macrophage accumulation. *Arterioscler. Thromb. Vasc. Biol.*, **31** (6), 1309–1316.

[36] Hinek, A., Braun, K.R., Liu, K., Wang, Y., Wight, T.N., (2004). Retrovirally mediated overexpression of versican v3 reverses impaired elastogenesis and heightened proliferation exhibited by fibroblasts from Costello syndrome and Hurler disease patients. *Am. J. Pathol.*, **164** (1), 119–131.

[37] Kang, I., Barth, J.L., Sproul, E.P., Yoon, D.W., Workman, G.A., Braun, K.R., Argraves, W.S., Wight, T.N., (2015). Expression of V3 Versican by Rat Arterial Smooth Muscle Cells Promotes Differentiated and Anti-inflammatory Phenotypes. *J. Biol. Chem.*, **290** (35), 21629–21641.

[38] Stellavato, A., Corsuto, L., D'Agostino, A., La Gatta, A., Diana, P., Bernini, P., De Rosa, M., Schiraldi, C., Karamanos, N.K., (2016). Hyaluronan Hybrid Cooperative Complexes as a Novel Frontier for Cellular Bioprocesses Re-Activation. *PLoS ONE*, **11** (10), e0163510.

[39] Joddar, B., Ramamurthi, A., (2006). Elastogenic effects of exogenous hyaluronan oligosaccharides on vascular smooth muscle cells. *Biomaterials*, **27** (33), 5698–5707.

[40] Kothapalli, C.R., Ramamurthi, A., (2009). Biomimetic regeneration of elastin matrices using hyaluronan and copper ion cues. *Tissue Eng. Part A*, **15** (1), 103–113.

[41] Cain, S.A., Baldwin, A.K., Mahalingam, Y., Raynal, B., Jowitt, T.A., Shuttleworth, C.A., Couchman, J.R., Kielty, C. M., (2008). Heparan sulfate regulates fibrillin-1 N- and C-terminal interactions. *J. Biol. Chem.*, **283** (40), 27017–27027.

[42] Ikeda, M., Naitoh, M., Kubota, H., Ishiko, T., Yoshikawa, K., Yamawaki, S., Kurokawa, M., Utani, A., Nakamura, T., Nagata, K., Suzuki, S., (2009). Elastic fiber assembly is disrupted by excessive accumulation of chondroitin sulfate in the human dermal fibrotic disease, keloid. *Biochem. Biophys. Res. Commun.*, **390** (4), 1221–1228.

[43] S.K. Karnik, B.S. Brooke, A. Bayes-Genis, L. Sorensen, J. D. Wythe, R.S. Schwartz, et al. A critical role for elastin signaling in vascular morphogenesis and disease. Development. 2003;130(2):411-23.

[44] Mack, C.P., Somlyo, A.V., Hautmann, M., Somlyo, A.P., Owens, G.K., (2001). Smooth muscle differentiation marker gene expression is regulated by RhoA-mediated actin polymerization. *J. Biol. Chem.*, **276** (1), 341–347.

[45] Miano, J.M., Long, X., Fujiwara, K., (2007). Serum response factor: master regulator of the actin cytoskeleton and contractile apparatus. *Am. J. Physiol. Cell Physiol.*, **292** (1), C70–C81.

[46] Gomez, D., Owens, G.K., (2012). Smooth muscle cell phenotypic switching in atherosclerosis. *Cardiovasc. Res.*, **95** (2), 156–164.

[47] Sibinga, N.E.S., Foster, L.C., Hsieh, C.-M., Perrella, M.A., Lee, W.-S., Endege, W.O., Sage, E.H., Lee, M.-E., Haber, E., (1997). Collagen VIII is expressed by vascular smooth

muscle cells in response to vascular injury. *Circ. Res.*, **80** (4), 532–541.

[48] Adiguzel, E., Hou, G., Mulholland, D., Hopfer, U., Fukai, N., Olsen, B., Bendeck, M., (2006). Migration and growth are attenuated in vascular smooth muscle cells with type VIII collagen-null alleles. *Arterioscler. Thromb. Vasc. Biol.*, **26** (1), 56–61.

[49] Yurdagul Jr., A., Finney, A.C., Woolard, M.D., Orr, A.W., (2016). The arterial microenvironment: the where and why of atherosclerosis. *Biochem. J.*, **473** (10), 1281–1295.

[50] Cherepanova, O.A., Pidkovka, N.A., Sarmento, O.F., Yoshida, T., Gan, Q., Adiguzel, E., Bendeck, M.P., Berliner, J., Leitinger, N., Owens, G.K., (2009). Oxidized phospholipids induce type VIII collagen expression and vascular smooth muscle cell migration. *Circ. Res.*, **104** (5), 609–618.

[51] Mack, C.P., (2011). Signaling mechanisms that regulate smooth muscle cell differentiation. *Arterioscler. Thromb. Vasc. Biol.*, **31** (7), 1495–1505.

[52] Wagenseil, J.E., Mecham, R.P., (2009). Vascular extracellular matrix and arterial mechanics. *Physiol. Rev.*, **89** (3), 957–989.

[53] Heinz, A., (2021). Elastic fibers during aging and disease. *Ageing Res Rev.*, **66**, 101255. https://doi.org/10.1016/j.arr.2021.101255.

[54] Hirano, E., Knutsen, R.H., Sugitani, H., Ciliberto, C.H., Mecham, R.P., (2007). Functional rescue of elastin insufficiency in mice by the human elastin gene: implications for mouse models of human disease. *Circ. Res.*, **101** (5), 523–531.

[55] Zhang, P., Huang, A., Ferruzzi, J., Mecham, R.P., Starcher, B.C., Tellides, G., Humphrey, J.D., Giordano, F.J., Niklason, L.E., Sessa, W.C., (2012). Inhibition of microRNA-29 enhances elastin levels in cells haploinsufficient for elastin and in bioengineered vessels–brief report. *Arterioscler. Thromb. Vasc. Biol.*, **32** (3), 756–759.

[56] Merrilees, M.J., Falk, B.A., Zuo, N., Dickinson, M.E., May, B.C.H., Wight, T.N., (2017). Use of versican variant V3 and versican antisense expression to engineer cultured human skin containing increased content of insoluble elastin. *J. Tissue Eng. Regen. Med.*, **11** (1), 295–305.

[57] Kothapalli, C.R., Gacchina, C.E., Ramamurthi, A., (2009). Utility of hyaluronan oligomers and transforming growth factor-beta1 factors for elastic matrix regeneration by aneurysmal rat aortic smooth muscle cells. *Tissue Eng. Part A*, **15** (11), 3247–3260.

[58] Keire, P.A., L'Heureux, N., Vernon, R.B., Merrilees, M.J., Starcher, B., Okon, E., Dusserre, N., McAllister, T.N., Wight, T.N., (2010). Expression of versican isoform V3 in the absence of ascorbate improves elastogenesis in engineered vascular constructs. *Tissue Eng. Part A*, **16** (2), 501–512.